Guardiola, C.; Pla Moreno, B.; Mora Pérez, J.; Lefebvre, D. (2019). Experimental determination and modelling of the diesel oxidation catalysts ageing effects. Proceedings of the Institution of Mechanical Engineers Part D Journal of Automobile Engineering. 233(12):3016-3029. https://doi.org/10.1177/0954407018814305

Experimental determination and modelling of the DOC ageing effects

Journal Title
XX(X):1–11

DOI: 10.1177/ToBeAssigned
www.sagepub.com/
SAGE

C. Guardiola[1] and B. Pla[1] and J. Mora [1] D. Lefebvre[2]

Abstract

After-treatment systems are necessary to respect the pollutant emissions thresholds specified by regulations. However, due to system ageing, the efficiency of the after-treatment system may decrease and affect the vehicle emissions during real driving conditions. To address this issue, the model presented in this article is based on the on-engine tests performed to a set of diesel oxidation catalysts with different ageing levels, through which the ageing process is characterized. Then, the model is able to simulate the light-off temperature and slip increase due to ageing, and it is applied to a WLTC for a new and a thermally aged catalysts.

Keywords

diesel oxidation catalyst, Diesel engine, ageing, model, emisisons, diagnostics

Introduction

Current worldwide regulations make necessary the use of after-treatment systems in combustion engines. However, these systems are deteriorated over time, so its performance has to be monitored by the on-board diagnostics (OBD) system to apply the corresponding measures[1–3]. Sensors-based and model-based methods have been widely used for this purpose[4–6]. In this article, a characterization of the deterioration processes and its impact on emissions is done to estimate the effects of Diesel oxidation catalysts (DOC) ageing. Then, a DOC model including ageing is presented.

The DOC is responsible for the oxidation of THC, CO and the volatile organic fraction VOF of PM, as well as the NO conversion into NO_2. These phenomena are mainly dominated by temperature, exhaust mass flow and exhaust gas composition. As reported by several authors like[7] and[8], the temperature range of activation, known as light-off temperature (LOT), determines the oxidation threshold, from which the DOC is able to oxidize. The catalytic functions of different emission species can have different LOT, being the light-off temperature of THC higher than the LOT of CO. In addition, forward and reverse LOT steps can affect this threshold, being NO_2 in high concentrations the main responsible for this variation in case of THC, due to inhibition effects[9,10]. Another important DOC characteristic is the accumulation process, in which THC are stored in the catalyst monolith while the DOC core temperature is under the light-off temperature[11].

In this article, no differentiation among THC species is taken into account, despite the fact that THC are composed of a large variety of hydrocarbons chains[12] which might affect the LOT.[13] and[14] considered two main groups: easy-to-oxidize, represented by C_3H_6, and difficult-to-oxidize compounds, in which chains with higher number of carbons are included, being $C_{10}H_{22}$ the most representative.[15] assumed THC as C_3H_6 for modelling purposes.

Despite the DOC capability of NO conversion into NO_2 does not strongly affect tail-pipe emission levels, it affects DPF passive regeneration and SCR reduction kinetics. NO_x chemical abatement in SCR can be represented by three reactions: NO reduction, NO_2 reduction and combined NO and NO_2 reduction. While the combined reaction is the fastest, the NO_2 reaction is the slowest, being a factor of 0.5 for NO_2 over NO_x when SCR shows the best reduction performance[16,17].

On-board ageing is considered to be a slowly varying process, which strongly depends on several factors like driving profile, frequency of DPF regenerations or fuel composition, specially if it contains sulfur. In this sense, thermal exposure of after-treatment systems to high temperatures is significant in general use conditions so that thermal mechanisms dominate over other processes like chemical poisoning. For this reason, thermal ageing is the main ageing process considered in this article.

In order to accelerate the effects of the ageing process for laboratory purposes, exposure of units to high temperatures is a common technique. In this sense, temperatures higher than 600°C cause a LOT increase of the catalyst, in which 10 to 16 hours cause an increase of 10°C in LOT[18]. In fact, the LOT increase of THC, CO and NO species has been analyzed by several authors like *Homayoun et al.*[19], *Bartley*[9] and *Nakane et al.*[20] by means of this artificial technique, showing also the effects of ageing on HC and CO emissions increase.

[1]CMT–Motores Térmicos, Universitat Politècnica de València, Valencia, Spain [2]PSA Peugeot Citroën, La Garenne-Colombes, France (e-mail: damien.lefebvre@mpsa.com)

Corresponding author:
Javier Mora, CMT–Motores Térmicos, Universitat Politècnica de València, Camino de Vera Sn, E-46022 Valencia, Spain
Email: jamopre1@mot.upv.es

A control-oriented model that includes ageing effects on THC and CO emissions, as well as an outline of the NO to NO_2 conversion, is presented in this article. 1D models are complex, with detailed equations for physical and chemical processes, so that the calibration of those models is subjected to a extensive and time-consuming testing campaign. Moreover, its accuracy may not be suitable for practical needs. For this reason, lumped models are valuable to reproduce functional processes of the catalyst. In this line, the functions of the presented control-oriented model are based on experimental tests that show in terms of slip the ageing effect on light-off temperature and THC accumulation capabilities. Authors like[21–23] have presented models for DOC including oxidation, but the novelty of this article is the inclusion of ageing.

The article is structured as follows: an outline of the model is presented in Section , the experimental set-up and tests are presented in Section , the ageing model is presented in Section and conclusions can be found in the last section. Finally, an appendix for model validation is included.

Modelling approach

The presented control-oriented model is composed of three main parts, which are the thermal model, the THC model and the CO model, as shown in Figure 1. Its aim is to estimate THC and CO slip emissions during normal engine operating conditions, rather than during excitation events like high post-injections used in DPF regeneration. The thermal model, described by the authors in[21], is a lumped model that considers a monolith, an external covering, a variable delay depending on the exhaust mass flow, and a sensor model. The thermal part, which represents the heat transmission and dynamics, is evaluated and validated in tests with load and engine speed steps to stress the system dynamics, as well as in NEDC and WLTC cycles. In case temperature sensor bandwidth is not enough to capture transient conditions, a data fusion technique could be applied as in[24]. The[21] model also includes a basic THC and CO slip model, which is upgraded in this article with experimental information and ageing functions. The considered functions are:

$$\dot{m}_{HC}^{out} = \beta_{HC} \cdot \dot{m}_{HC}^{in} \tag{1}$$

$$\dot{m}_{CO}^{out} = \beta_{CO} \cdot \dot{m}_{CO}^{in} \tag{2}$$

where $\dot{m}_{HC}^{in}$ is the mass flow of entering HC, β_{HC} is a slip factor outlined in equation 3, $\dot{m}_{HC}^{out}$ is the mass flow of HC released, $\dot{m}_{CO}^{in}$ is the mass flow of entering CO, β_{CO} is a slip factor outlined in equation 4, $\dot{m}_{CO}^{out}$ is the mass flow of released CO. The capacity of the DOC for accumulating HC[25] is also modelled and the slips β_{HC} and β_{CO} are considered to be the ratio of species escaping from the DOC over those entering in it. Equations 3 and 4 show which are the model inputs:

$$\beta_{HC} = f(T_{in}, \dot{m}_{HC}^{in}, m_{HC}^{acc}, LOT_{HC}, \xi) \tag{3}$$

$$\beta_{CO} = f(T_{in}, \dot{m}_{CO}^{in}, LOT_{CO}, \xi) \tag{4}$$

where T_{in} is the DOC inlet temperature, m_{HC}^{acc} is the accumulated HC and LOT$_HC$ LOT$_CO$ are the initial LOT values of HC and CO, respectively. While T_{in} and $\dot{m}_{HC}^{in}$ are the model inputs, m_{HC}^{acc} is a state and LOT and ξ are relevant tunable parameters. Experimental tests are used to characterize how the DOC operates and how it is affected by ageing. In this line, the modelled functions are selected taking into account an ageing perspective, so that an ageing factor ξ allows progressively switching from new to aged behaviours.

The combination of simple equations allows having a model that includes species slip, oxidation, HC accumulation and light-off temperature, since a compromise between calibration complexity, functions flexibility and process physical description is necessary. As a result, the model is able to set a relationship among ageing, LOT and emissions increase. In this sense, if an indirect technique like LOT estimation were used for DOC diagnostics, the on-board estimated value could be related to a previously off-line associated emissions increase and therefore a malfunction indicator light (MIL) could be shown if regulation emissions are overcome.

Experimental set-up and tests

A series of experimental tests was carried out in order to analyse the performance of several DOCs with different ageing levels. A direct injection Euro 5 diesel engine was used as a gas generator to feed DOCs with exhaust gas in conditions that stressed their capacities. Moreover, dynamic tests like the WLTC were also done for each DOC. The engine, mounted in an engine test bench, was mainly composed of a high pressure common-rail fuel injection system, an Exhaust Gas Recirculation (EGR) system and a Variable Geometry Turbine (VGT). The exhaust line was composed of a DOC, as the only after-treatment system, and several exhaust gas measurement systems.

The engine injection strategy had to be modified in order to inject raw fuel in the exhaust line to feed DOCs with THC, for which late post-injections were the key parameter. For this purpose, a bypass was done to the ECU through an ETAS 910, while a rapid prototyping system dSpace real time Microautobox II was used as a signals generator for post-injections and for the NTC temperature sensors measurement acquisition. The engine was controlled from a Horiba Stars PC, to which different general engine operating signals were connected.

Gases composition, specifically THC, CO, NO and NO_x, were measured by means of a Horiba Mexa 7100 series exhaust gas analyser, as shown in Figure 2. The THC were measured through a flame ionization detector heated vacuum-type (HFID), the CO were measured by means of a non-dispersive infra red (NDIR) procedure, while the NO and NO_x were measured with the Heated Chemiluminescence Detector (HCLD). These measurement processes induced response times from 1s to 3s that could not be avoided in dynamic tests like the NEDC or the WLTC. The THC are measured in CH_4 equivalent ppm, so the conversion from gas concentration to gas flow was done through the following equation:

$$HC[kg/s] = HC[ppm] \cdot \dot{m}_{exh}[kg/s] \cdot \frac{M_{CH_4}}{M_{air}} \cdot 10^{-6} \tag{5}$$

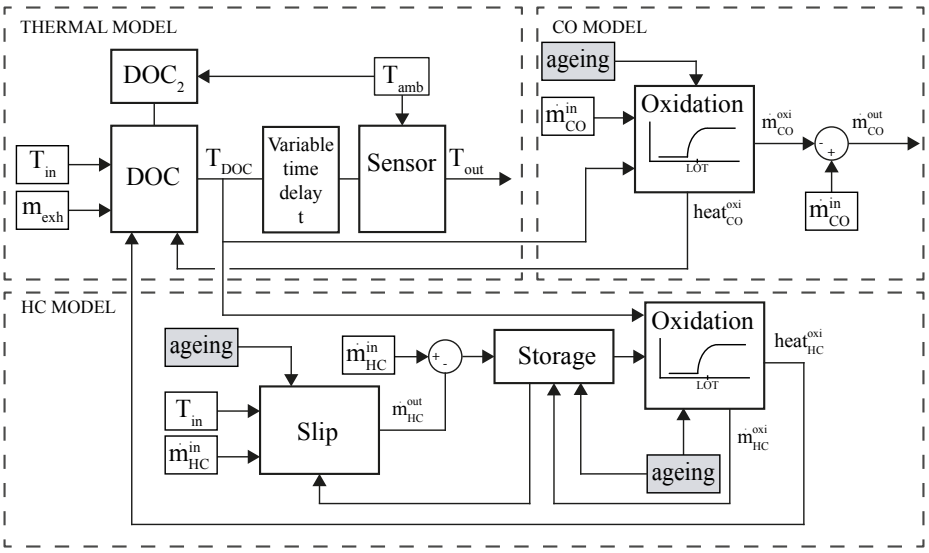

Figure 1. DOC model layout.

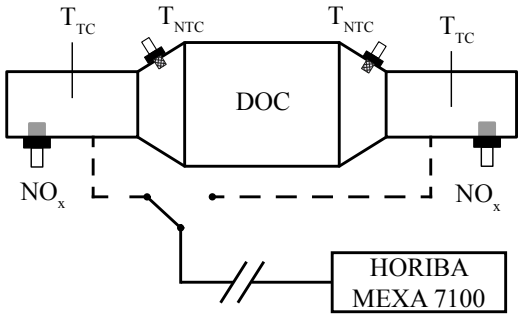

Figure 2. Scheme of the measurement layout.

where $\dot{m}_{exh}$ is the exhaust mass flow, M_{air} and M_{CH_4} are the molecular weights of air and methane, respectively, and HC is the species concentration measured by the gas analyzer.[26] proposes a non-linear fitting procedure to estimate DOC upstream THC from post-injections in accordance with the injection timing, although measured THC are used in this article.

Two on-board NO_x sensors were used in company with NO and NO_x measurements from the gas analyzer to account for the NO to NO_2 conversion of the catalyst. Figure 3 shows the result of the NO_x sensors calibration with the gas analyzer measurements. A linear correction function with 0 origin was fit to 38 steady-state measured points from 50 ppm to 1600 ppm, which is the saturation value for the NO_x sensor. The correction functions are:

$$NO_{x,sen}^{us,corr} = 0.9936 \cdot NO_{x,gasanalyzer}^{us} \quad (6)$$

$$NO_{x,sen}^{ds,corr} = 1.032 \cdot NO_{x,gasanalyzer}^{ds} \quad (7)$$

where $NO_{x,gasanalyzer}$ corresponds to the Horiba gas analyzer measurement and $NO_{x,sen}^{us,corr}$ and $NO_{x,sen}^{ds,corr}$ correspond to the upstream and downstream NO_x sensors measurements, respectively. Then, NO_x measurements are corrected to correspond to the gas analyzer equivalent measurement.

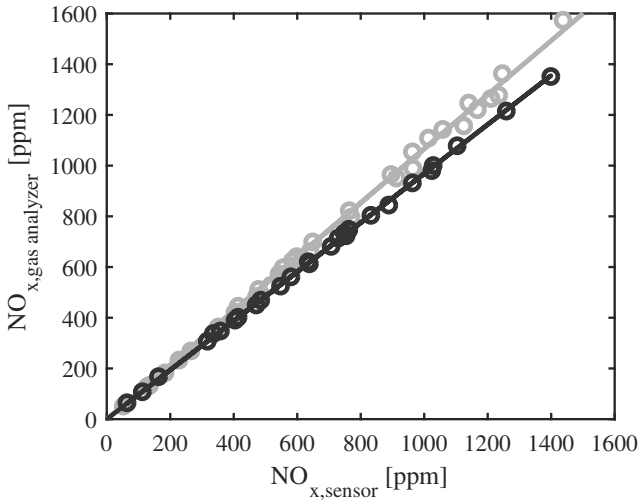

Figure 3. NO_x sensors calibration, where circles are experimental values and lines are correction functions. Upstream sensor — Downstream sensor.

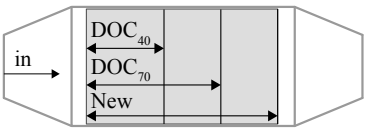

Figure 4. Scheme of the new, DOC_{70} and DOC_{40} catalyst lengths.

Catalysts

A set of 6 DOCs was used in this article. Except for a non-impregnated catalyst, the rest had the same properties in brand new conditions. Then, different ageing procedures were applied to each one, which are described next:

New DOC It is the basic DOC, composed of a ceramic monolith, whose washcoat impregnation is a mixture of Pt and Pd and an external isolation layer.

Nominal DOC It is a DOC whose operation conditions did not exceed higher temperatures than 600°C during long phases, i.e. smooth ageing conditions.

Aged DOC It has an artificial ageing procedure at 800°C during 25h. Thermal ageing is considered to be a valid ageing method [19,27] for DOCs.

DOC$_{70}$ It is the new DOC but with 70% of the catalyst monolith length. A cut process was applied to this DOC in order to reduce the effective length. Due to the homogeneous properties of DOCs, the effective length is considered to be a measure of the effective area. It keeps the external isolation layer.

DOC$_{40}$ It is the new DOC but with 40% of the catalyst monolith length, i.e. it followed the same cutting process of the DOC$_{70}$.

Non-impregnated DOC It was used as a completely faulty DOC, which lacks of catalytic capacities and only behaves as a regenerative heat exchanger.

The DOC$_{70}$ and the DOC$_{40}$ were obtained in two phases from the new DOC following the same mechanical process, which consisted in opening the external canning and removing a slice of 30% length of the catalyst monolith. In the first phase, after removing the first 30% slice, the DOC$_{70}$ was obtained. Then, after doing all necessary tests, the process was done again for the DOC$_{40}$, removing another 30% slice of the monolith. The portion of the monolith that was removed was at the downstream part, in order to maintain the distance from the cylinders to the DOC inlet and do not affect the temperature of the exhaust gases entering the DOC. Figure 4 represents this structure. Then, the DOC canning was welded again, so that the external dimensions of the brand new DOC were kept. Next, performance of the different DOCs was evaluated through a series of experiments that stress the main operation characteristics, which are the light-off temperature, the HC accumulation and the HC and CO slip.

Light-off temperature test

The light-off temperature is a characteristic that affects HC, CO and NO species concentrations. Some authors like [28] and [18] define the LOT as the temperature at which 50% of the incoming considered species are oxidized, since LOT does not act as a real binary threshold. Figure 5 shows the test done to estimate the LOT of HC, CO and NO species. Medium plots of Figure 5 allow observing the effect of LOT for HC, CO and NO species concentrations. This test starts with both DOC up- and downstream temperatures below 130°C, which is a low enough temperature under LOT. Then, load steps of 2 minutes are applied to slowly increase the temperature, about 20°C each approximately. In order to ensure an enough exothermic event, in which the downstream temperature clearly increases over the upstream, a post-injection pulses train of 3 mg/str, like the shown in Figure 6, was continuously applied at the start of the load steps, so the DOC is continuously being filled with HC.

In case of HC, an accumulation process can be observed as HC$_{out}$ increases until the LOT is reached, in which point a noticeable temperature increase takes place. From this temperature, the oxidation process empties the accumulated

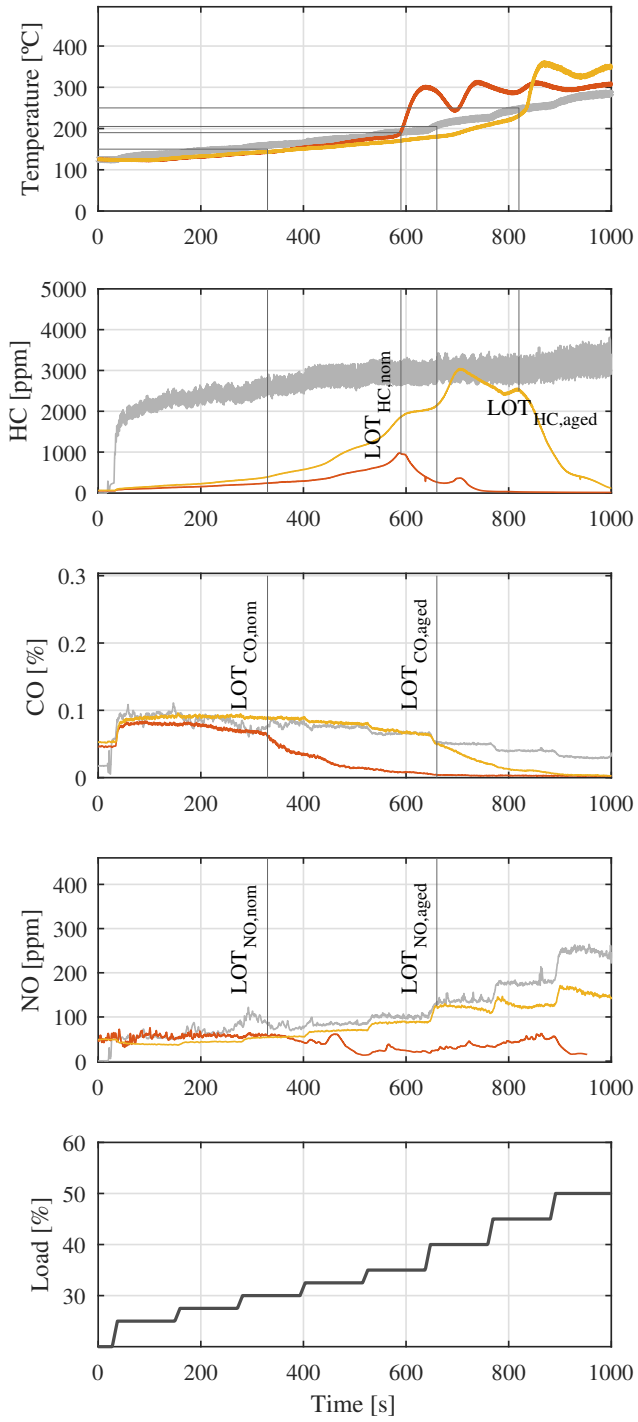

Figure 5. Results of the light-off temperature test for the new and aged DOCs. Upstream measurements. New DOC downstream measurements. Aged DOC downstream measurements.

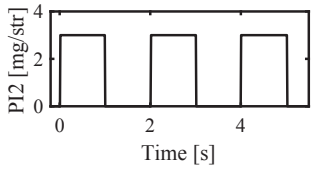

Figure 6. Pulses train of late fuel post-injections.

Table 1. Light-off temperature test results.

Catalyst	New	Nom	Aged	DOC_{70}	DOC_{40}	No-imp
LOT_{HC}	190	190	250	190	190	-
LOT_{CO}	150	150	205	150	150	-
LOT_{NO}	150	150	205	150	150	-

HC in the catalyst and a $[HC]_{out}$ decrease is observed. The step from HC accumulation to oxidation can therefore be observed through an exothermic increase of temperature and with a decrease of HC_{out}. This behaviour can be observed for both new and aged DOCs, being the LOT of each one at a different temperature. In the case of the aged DOC, the HC accumulation even reaches the saturation point, since $[HC]_{out}$ are similar to the $[HC]_{in}$. If HC oxidation was not high enough to observe differences in temperature, the LOT could not be evident, since an inherent difficulty of differentiating between accumulation and oxidation exists observing HC_{in} and HC_{out} concentrations.

In case of NO and CO, the LOT estimation is simpler, since the decrease of DOC_{out} species concentrations marks the temperature at which the light-off is reached. $[CO]_{out}$ is maintained constant, being $[CO]_{in}$ equal to $[CO]_{out}$ until its LOT is achieved. This effect shows the lack of CO accumulation capabilities of the DOC. In case of NO, an analog effect happens. The light-off temperature can be appreciated through a decrease in concentration, although oxidation is not complete in this case. As it can be also observed, LOT for CO and NO is, in both new and aged cases, lower than for HC.

Table 1 shows the results of the LOT tests for all DOCs. As the cut procedure does not affect the activation energy, the cut DOCs have the same LOT, while the LOT of the thermally aged DOC has increased up to 250°C. Note that oxidation starts inside the DOC at a temperature that may differ from the inlet gas temperature, since the outlet temperature is lower due to thermal losses. However, as the DOC monolith temperature is not measured on-board, the light-off temperature is characterised by the upstream temperature sensor.

HC accumulation test

The objective of the HC accumulation test is to measure how much HC a DOC is able to store, and characterize how HC slip increases as the DOC is being filled. For this purpose, the DOC is filled with HC from engine post-injections until it is saturated, i.e. the downstream measured HC are stabilized and equal to the HC measured upstream. This test is composed of three phases, as identified in Figure 7:

1. Emptying phase: The engine runs at a point in which the temperature is sufficiently high to ensure the removal of any possibly stored HC. Engine speed is shown at the bottom plot of Figure 7.

2. Temperature stabilization phase: From this phase, the engine runs at steady-state conditions until the end of the test. It is a transition phase, in which DOC temperature is continuously decreasing until the downstream measurement falls below the LOT value, in which moment post-injections start.

3. Accumulation phase: It is the post-injections phase, during which post-injection pulses of 3 mg/str like the presented in Figure 6 are being continuously applied until the downstream HC measurement reaches the steady HC upstream measurement.

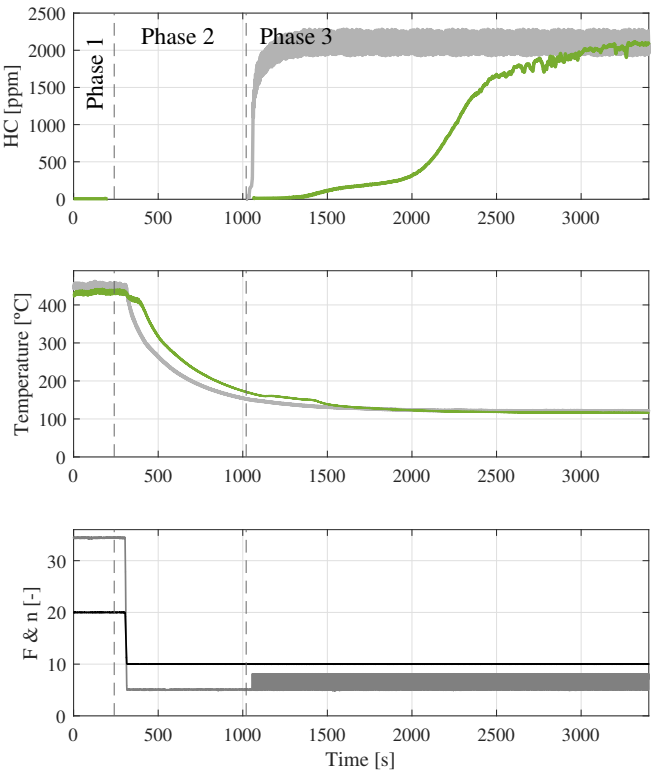

Figure 7. Results of the HC accumulation test for the nominal DOC. Top and medium plots: Upstream measurements Nominal DOC downstream measurements. Bottom plot: Fuel post-injection in mg/str Engine speed n/100 in rpm

Post-injections, shown at the bottom plot of Figure 7, start when DOC temperature is below LOT. However, a slight change of slope in temperature after the start of post-injection between 1000 and 1500s can be appreciated in Figure 7, which is due to the CO oxidation, whose LOT is lower than for the HC.

Results of the accumulation test applied to each DOC are shown in Figure 8. The behaviour of the catalysts is the same for all: HC slip increases as the DOC is being filled with HC. It can be also appreciated how as the DOC ages, its slip increases, while its ability to filter the post-injection pulses decreases.

The different ageing of the DOCs has impact on the slip increase, since the brand new DOC is able to accumulate HC with only a slight increase on slip, while the nominal and aged DOCs have more slip, following both a similar trend: they have an initial strong increase, followed by a smoothed slope. The DOC_{70} follows a similar trend than the new catalyst, but it gradually starts increasing its slip before. Then, the DOC_{40} is the less capable of storing HC, so its slip increases faster than for the others.

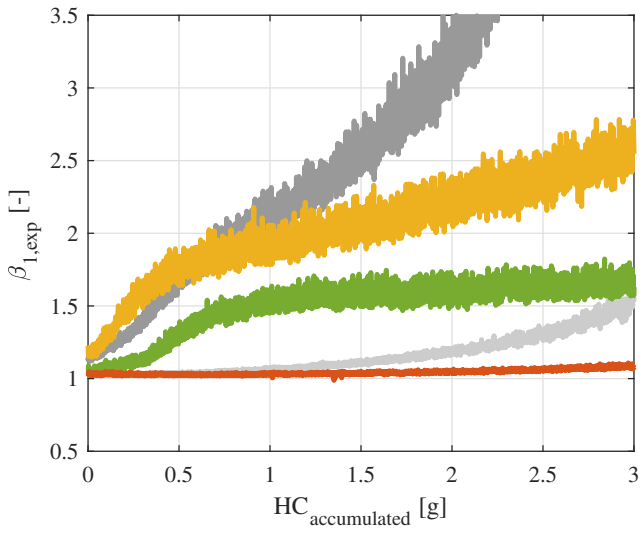

Figure 8. Experimental results of the HC accumulation test. New DOC Nominal DOC Aged DOC DOC_{70} DOC_{40}.

DOC active model

Figure 9 shows a test used to describe the basic principles of the HC and CO slip model, with the experimental behaviour of nominal and aged pieces. This test embraces a wide range of loads and engine speeds of the engine, being therefore variety in temperatures and exhaust mass flows. Light-off temperature effects can be appreciated from 500 s approximately, when slip is reduced for both HC and CO. Despite having different LOT, the step is big enough to overcome both LOT almost at the same time. In case of HC, the slip for the aged catalyst is higher than for the nominal until the LOT is reached, from which point both slips are similar. In this line, CO slip has a similar behaviour, being the initial part at cold conditions with higher slip for the aged unit, and being the warm part with high efficiency for both catalysts. Model coefficients are shown in Table 2.

HC and CO oxidation model

Traditional chemical modelling for oxidation reactions like 8 and 9 follows an Arrhenius reaction rate[29]. However, the reaction rate in this article is modelled through equation 10, which is a more flexible function, and allows setting the interval range from no oxidation to oxidation, the increasing shape and the maximum reaction rate.

$$CH_4 + 2O_2 \rightarrow CO_2 + 2H_2O \tag{8}$$

$$2CO + O_2 \rightarrow 2CO_2 \tag{9}$$

$$\chi = \chi_{max} + \left(\chi_{max}^{n} + \frac{(\chi_{max} - \chi_{min})^n \cdot (T_{DOC} - LOT)^n}{\Delta LOT^n} \right)^{n^{-1}} \tag{10}$$

where χ is the oxidation rate of HC or CO. Increasing and decreasing oxidation rates are limited to avoid too fast DOC emptying processes:

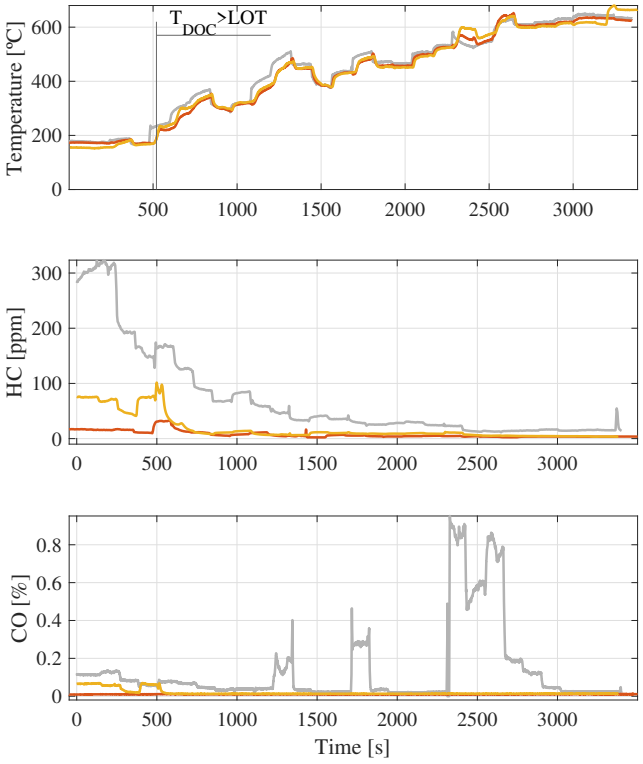

Figure 9. Reference test with HC and CO to develop the model. Upstream measurements New DOC downstream measurements. Aged DOC downstream measurements.

Table 2. Model coefficients.

HC Oxidation	
LOT_{HC}	HC light-off temperature
ΔLOT_{HC}	HC temperature activation interval
n_{HC}	HC shape coefficient for temperature activation interval
$\chi_{HC,min}$ $\chi_{HC,max}$	Minimum and maximum HC oxidation rates
$\left(\frac{d\chi_{HC}}{dt}\right)_{min}$ $\left(\frac{d\chi_{HC}}{dt}\right)_{max}$	Minimum and maximum activation and deactivation rates for HC oxidation
HC accumulation and slip	
a_1 to a_4	$slip_0$ function coefficients
s, a and m_{HC}^{ref}	$slip_1$ function coefficients, which are affected by A_eff
A_{eff}	Effective area
CO oxidation	
LOT_{CO}	CO light-off temperature
ΔLOT_{CO}	CO temperature activation interval
n_{CO}	CO shape coefficient for temperature activation interval
$\chi_{CO,min}$ $\chi_{CO,max}$	Minimum and maximum CO oxidation rates
$\left(\frac{d\chi_{CO}}{dt}\right)_{min}$ $\left(\frac{d\chi_{CO}}{dt}\right)_{max}$	Minimum and maximum activation and deactivation rates for HC oxidation

$$\left(\frac{d\chi}{dt}\right)_{min} < \frac{d\chi}{dt} < \left(\frac{d\chi}{dt}\right)_{max} \quad (11)$$

Then, the oxidation reactions are limited by the available oxygen, the available HC or CO, and a maximum oxidation rate.

HC slip model

T_{in}, $\dot{m}^{in}_{HC}$ and m^{acc}_{HC} are the factors influencing this model function, since it is experimentally observed that the slip in cold conditions is lower than in warm conditions, while $\dot{m}^{in}_{HC}$ is related to the residence time of the THC in the DOC and follows the idea of the higher the mass flow the higher the slip. Regarding the amount of THC stored in the DOC, the higher the amount of THC stored, the lower the ability of the DOC to capture more THC and therefore the higher the slip. In the limit, when the DOC is completely saturated of THCs, its ability to retain more THC is 0, and then a slip of 100% appears, as shown in Figure 7.

Slip is modelled through the function β_{HC}, being β_0 a function that depends on $\dot{m}^{in}_{HC}$ and T_{in}, and β_1 a factor that depends on m^{acc}_{HC}. β_0 represents the basic slip of the DOC, while β_1 adds to this basic slip the increase due to accumulation as a factor whose value is higher than 1.

$$\beta_{HC} = \beta_0(T_{in}, \dot{m}^{in}_{HC}) \cdot \beta_1(\dot{m}^{acc}_{HC}) \quad (12)$$

where β_0 is a quadratic polynomial:

$$\beta_0 = a_1 \cdot \dot{m}^{in}_{HC} + a_2 \cdot T_{in} + a_3 \cdot T^2_{in} + a_4 \cdot \dot{m}^{in}_{HC} \cdot T_{in} \quad (13)$$

where a_i are calibrable coefficients. Figure 10 shows the experimental versus modelled relation between $\dot{m}^{in}_{HC}$ and T_{in}, where dots represent experimental measurements and contour lines represent modelled slip. These results are obtained by computing steady state points measured with the nominal DOC and fitting the parameters in equation 13 to the experimental data. Due to the complexity of the HC reaction in the DOC, non-linear fitting procedures and mapping are used in modelling[30].

The effect of m^{acc}_{HC} on the slip is modelled through the function β_1, shown in Figure 11. Results of the accumulation process versus slip of Figure 8 show that when the DOC does not have HCs stored, m^{acc}_{HC}=0, its slip increases linearly as it is progressively filled with HCs. Then, some reduction in the slope between m^{acc}_{HC} and slip is observed as m^{acc}_{HC} increases. Finally, as the amount of HC stored reaches the maximum capacity of the DOC a sudden increase happens. According to the previous description, the β_1 factor is defined as a piecewise function containing a linear and an exponential term modelling the effect of m^{acc}_{HC} on the slip:

$$\beta_1 = min(\beta_{1,slope}, \beta_{1,exp}) \quad (14)$$

where $\beta_{1,slope}$ and $\beta_{1,exp}$ are the functions that describe the slip due to HC accumulation, shown experimentally in Figure 8. This behaviour is modelled through equations 15 and 16, represented in Figure 11 and described next:

$$\beta_{1,slope} = 1 + s \cdot m^{acc}_{HC} \quad (15)$$

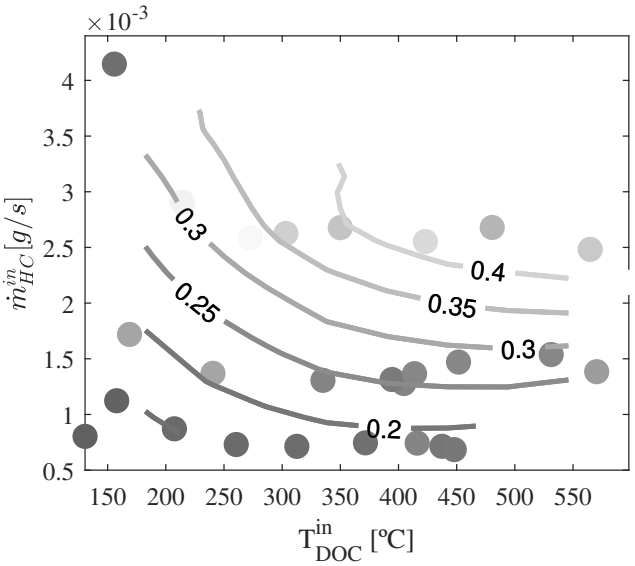

Figure 10. Results of the non-linear fitting of the slip function $slip_0$, where z values correspond to slip values. Dots stand for experimental measurements, while lines stand for modelled values.

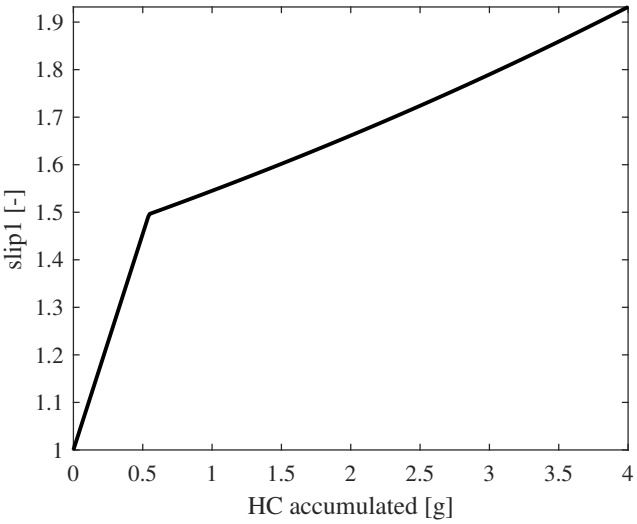

Figure 11. Graphical representation of the β_1 function.

where s is the slope of function $\beta_{1,slope}$, while the constant is set to 1 to leave the THC slip as β_0 when there is no HC accumulation.

$$\beta_{1,exp} = a + e^{\frac{m^{acc}_{HC}}{m^{ref}_{HC}}} \quad (16)$$

where a and m^{ref}_{HC} are calibrable parameters. The m^{ref}_{HC} parameter is related with the HC storage capability of the DOC, which is related with its ageing state.

CO slip model

The CO model is simpler than the HC model, since CO is not accumulated in the catalyst. In this case, the CO oxidation curve points which is the slip, since if CO are not being oxidized, then they are being released.

Model application

Since the model is oriented to simulate tests like the NEDC or the WLTC, rather than engine extreme conditions of load and speed or high post-injections, the model is applied to these kind of tests. Therefore, while LOT and slip tests are performed separately, the identification of the active model parameters is globally done using a WLTC. Then, the application of the model to a WLTC with the parameters from the resulting calibration is shown in Figure 16. In case of high post-injections, like during DPF regeneration conditions, a more detailed heat transmission and heat release model would be required.

Model calibration consists of two main steps: passive model calibration and active model calibration. Passive model calibration is done using the non-impregnated DOC through a least squares error minimization routine combined with manual tuning to provide the optimization function with good initial values. Then, the HC slip function is calibrated following a similar procedure, in which manual tuning and parametric studies are also required. In particular, the CO model is manually tuned, due to the saturation periods, which complicate the use of an optimization routine. For the LOT, the value obtained from experiments of Figure 5 in section , whose results are shown in Table 1, are used for each catalyst.

When fitting slip coefficients, engine exhaust flows from the WLTC cycle are higher than for the HC accumulation tests and therefore DOCs are filled faster. Then, constant values for this functions have been selected as a compromise solution for the engine operating ranges of the NEDC and WLTC tests.

As the engine load and catalyst temperature increases, some of the stored THCs may be released without being oxidized, resulting in a decrease in conversion. However, this effect is not normally observed in light-off small-scale[7] events. Therefore, this model is not appropriated for large post-injections, but it is to be used in conventional use cases. Note that slip and LOT are treated as independent processes, so that the effective area is not used to characterize the LOT.

The model is applied to a WLTC test in Figure 16, in which results for temperature and cumulative efficiencies $\eta_{cumulative}$ of HC and are shown. The HC excitation is high enough as a result of engine-raw emissions, since the engine operates in zones near high HC emissions. It can be seen that the passive model of[21] captures the heat transference and dynamics, whilst the HC and CO models are able to represent the DOC-outlet emissions. The following set of equations is used to evaluate the model performance:

$$eff_{exp} = 1 - \frac{\int \dot{m}^{out,exp}}{\int \dot{m}^{in}} \tag{17}$$

$$eff_{mod} = 1 - \frac{\int \dot{m}^{out,mod}}{\int \dot{m}^{in}} \tag{18}$$

$$\epsilon = \left| \frac{\int \dot{m}^{out,exp} - \int \dot{m}^{out,mod}}{\int \dot{m}^{in}} \right| \tag{19}$$

where eff_{exp} is the experimental efficiency, eff_{mod} is the modelled effiency, ϵ is the efficiency error and $\dot{m}$ is the mass flow of either HC or CO, whose results are shown in Table 3. Unfortunately, the accumulated HC cannot be validated, since it is a non-measurable state.

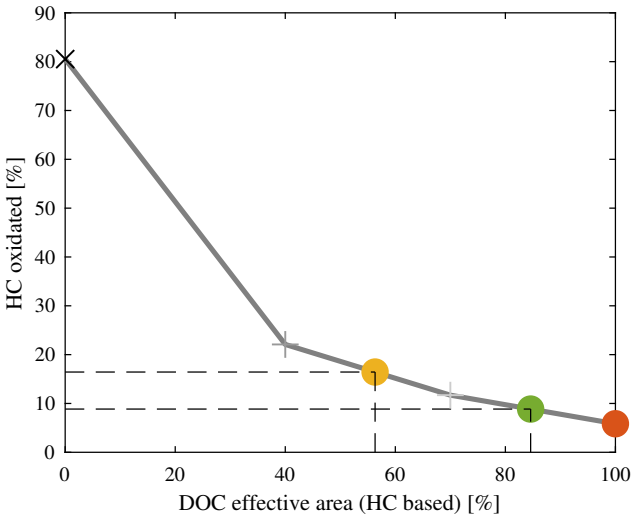

Figure 12. Experimental results for the effective area determination, where x is the non-impregnated DOC, + is the DOC_{40}, ● is the aged DOC, + is the DOC_{70}, ● is the nominal DOC and ● is the new DOC

The validation of the model has to be done with the available data from the catalysts available, so that efficiency results for the new and nominal catalysts are presented in Table 3. With the application of the model, the new DOC has an error of 1.4% for HC and 3.5% for CO, while the nominal DOC has an error of 0.2% for HC and 6.7% for CO. In both cases, the error obtained is acceptable, being slightly lower for HC than for CO.

Ageing modelling

Experimental data from the cut DOCs is used to define a parameter that characterizes the ageing level of a DOC. This approach allows defining an ageing parameter in terms of effective area A_{eff}, despite the mixed effect of residence time and loss of monolith efficiency. Then, according to their HC emissions in a WLTC, the effective area of the nominal and aged DOCs is set with respect to the new, the DOC_{70}, the DOC_{40} and the non-impregnated DOC, as shown in Figure 12. In this figure, 0% is referenced to the non-impregnated DOC, in which DOC-outlet HC emissions are equal to the engine-raw, while 100% corresponds to the new DOC. In this line, when the nominal DOC has an equivalent effective area of 85%, this value is reduced to 56% for the aged DOC. The effect of ageing in the oxidation function is modelled by means of the LOT for both HC and CO, using the values presented in Table 1.

Since results show that new and aged DOCs present similar slip at warm conditions, the main differences are appreciated during cold phases, i.e.: during HC accumulation, so that the ageing effect on HC slip is taken into account with the accumulated HC. Therefore, the HC slip ageing function is introduced to equation 12, and the expression for the slip becomes:

$$\beta_{HC} = \beta_0(T_{in}, \dot{m}^{in}_{HC}) \cdot \beta_1(m^{acc}_{HC}, A_{eff}) \tag{20}$$

where β_1 function (eq. 14) is upgraded with ageing. For this purpose, the WLTC test is fitted in terms of temperature,

Table 3. Efficiency of DOCs and model errors.

	eff_{exp} [%]	eff_{mod} [%]	ϵ [%]
New: HC	93.8	92.4	1.4
New: CO	83.5	80	3.5
Nominal: HC	91.1	92.3	0.2
Nominal: CO	76.6	93.3	6.7
Aged: HC	83.6	83.6	0
Aged: CO	61.9	53.9	8

HC slip and CO slip for each catalyst and the resulting coefficients are then combined with the effective area:

$$s = A_{eff} \cdot c_1 + c_2 \tag{21}$$

$$a = A_{eff} \cdot c_3 + c_4 \tag{22}$$

$$HC_{ref} = (A_{eff} \cdot c_5)^{-1} \tag{23}$$

where coefficients of the linear functions a and s (c_1 to c_4) are fitted with a minimum least squares error routine to a first order polynomial, while the coefficient c_5 is obtained by means of a parametric study, choosing the value of the coefficient that minimises the difference between the HC_{ref} value obtained from the fitting of the experimental results to the model and the result of applying equation 23. Note that parameters of cut DOCs were manually tuned focusing on low flow intervals, since differences in behaviour were observed at medium to high flows due to different residence times. Figure 13 shows the fitting of the model coefficients identified experimentally for the different DOCs and the correlations 21-23.

The maximum storage capacity also decreases as the DOC ages, although DOCs are able to store much more HC than those accumulated during WLTC conditions due to engine-raw emissions. Figure 17 shows the result of the model including ageing in the WLTC, whose performance is shown in Table 3. It can be observed how the DOC efficiency for HC fits well in average for the three catalysts, while the CO error increases up to 8 %.

Finally, the ageing factor parameter ξ is presented as the global ageing factor that relates A_{eff} and LOT, being 0 for the new DOC and 1 for the aged DOC. In this line, two reference catalysts lead to a first order relation between ξ and both LOT and A_{eff}, where ξ=0 corresponds to the new DOC and ξ=1 corresponds to the artificially aged DOC. In this sense, more intermediate units could lead to a more complex function, so the following equations represent this relation in the case presented:

$$LOT_{HC} = 14.93\,\xi + 47.31 \tag{24}$$

$$LOT_{CO} = 58.82\,\xi + 127.65 \tag{25}$$

$$A_{eff} = -43.48\,\xi - 98.7 \tag{26}$$

Impact of ageing on the NO to NO_2 conversion

An outline of the effect of ageing on the NO to NO_2 conversion is described next. As seen in Figure 5 of Section for the LOT, NO oxidation into NO_2 is affected by ageing. Figure 14 shows that the averaged value of the NO to NO_2 conversion is also affected by ageing. Since upstream and downstream NO signals could not be measured at the same time with the gas analyzer, the NO to NO_2 is analyzed comparing the NO to NO_x ratio, by means of equation 27.

$$\gamma = \frac{NO^{ds}}{NO_x^{us}} \tag{27}$$

The dynamic test shown in Figure 14 corresponds to a warm phase of the WLTC, in which the monolith temperatures are comprised between 200°C and 400°C. During this part of the test, the averaged conversion for the new DOC is 0.73, while the averaged conversion for the aged DOC is reduced to 0.4.

The DOC ageing has another effect on the NOx species with regards to its accumulation capabilities in cold phases, which is represented in Figure 15. During the initial 45 seconds, the new DOC accumulates NO_x, since the NO_x^{ds} signal is sensitively lower than the NO_x^{us} signal. Then, a release phase can be observed during 80 and 90 seconds. When analyzing the same effect in the aged DOC, this accumulation / release effect is not present, since both NO_x^{us} and NO_x^{ds} signals are similar during the first 45 seconds, and no release phase can be observed.

Conclusions

The DOCs ageing effect on emissions is characterized and modelled in this article. The results of a set of experimental tests is used to assess the main operation characteristics like the light-off temperature and the slip. The light-off temperature results of the HC, CO and NO emissions is presented and the accumulation capabilities are characterized for the HC species. An effective area, obtained with cut catalysts is used to characterize the HC slip ageing. Then, the model functions are developed to describe those processes.

The model, which groups these functions, is developed from the basis of a passive thermal lumped model, and is then applied to a WLTC for the new and aged catalysts. Due to the simple model approach, it is not suitable in case of high heat transmission phases. Thus, this model allows performing simulations in WLTC-like conditions.

An outline of the ageing effect of DOC on NO to NO_2 conversion is also presented with the conversion capacity and the LOT.

Acknowledgements

This research has been partially financed by the Spanish Ministerio de Economía y Competitividad, through project TRA2016-78717-R.

References

1. Posada F and German J. Review of LDV OBD requirements under the European, Korean and Californian emissions

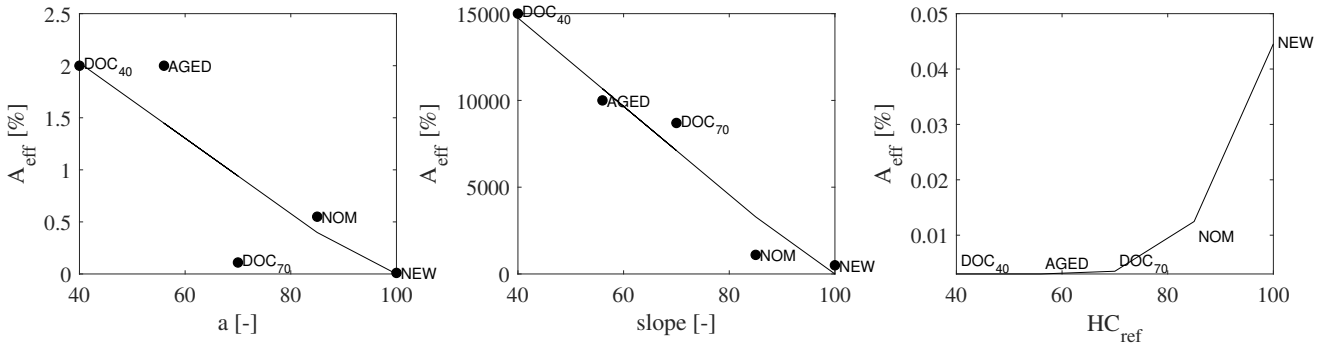

Figure 13. Results of the effective area for the HC slip ageing modelling.

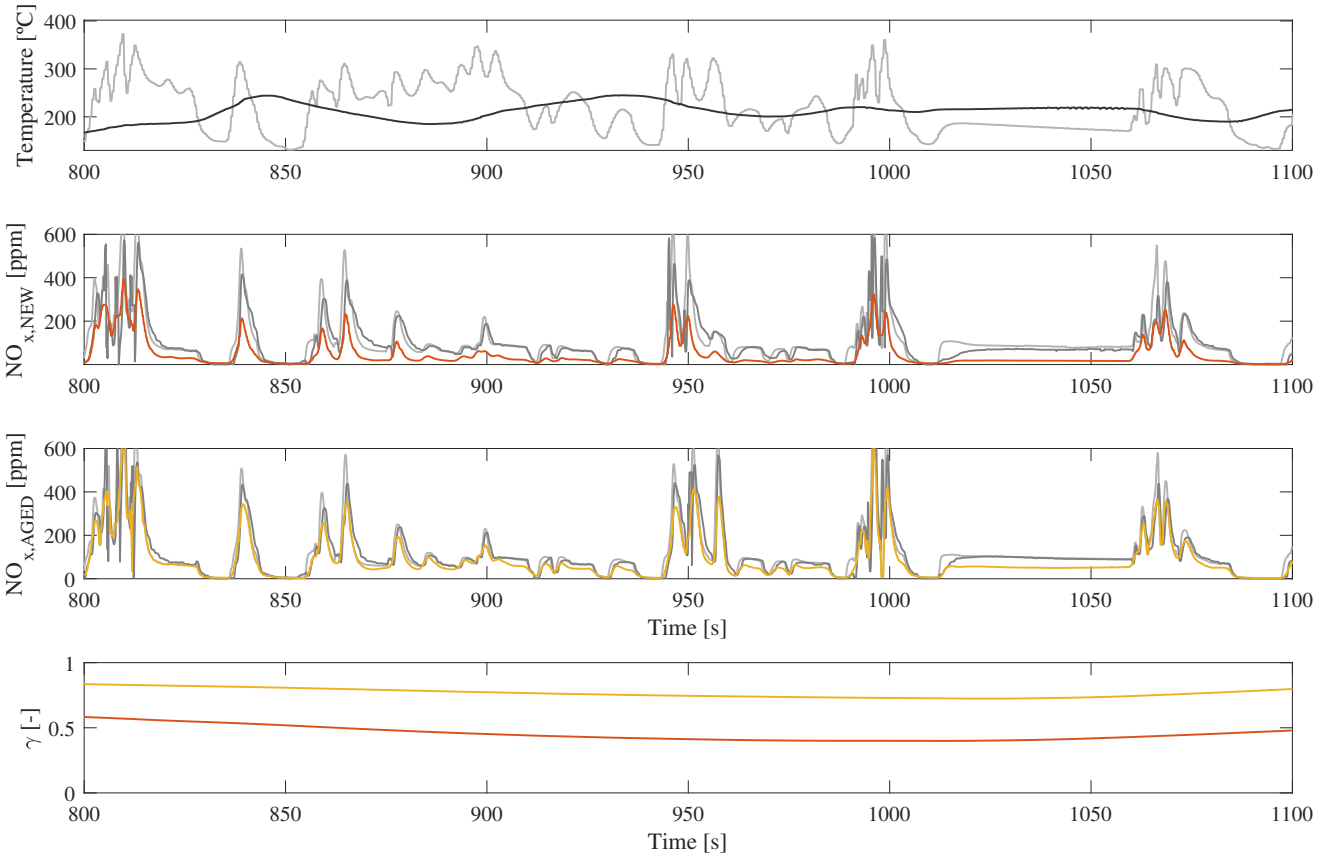

Figure 14. Measured NO_x signals during a warm phase of the WLTC. Top plot: Upstream temperature — Downstream temperature. Medium plots: $NO_{x,in}$ — $NO_{x,out}$ — $NO_{out,new}$ — $NO_{out,aged}$. Bottom plot: Averaged NO_{new} conversion — Averaged NO_{aged} conversion.

programs. *The international council on clean transportation* 2016; .

2. Alkemade UG and Schumann B. Engines and exhaust after treatment systems for future automotive applications. *Solid State Ionics* 2006; 177(26-32): 2291 – 2296.
3. Johnson T. Vehicular emissions in review. *SAE International Journal of Engines* 2016; 9(2): 1258–1275. DOI:https://doi.org/10.4271/2016-01-0919.
4. Nieuwstadt MV, Upadhyay D and Yuan F. Diagnostics for diesel oxidation catalysts. In *SAE Technical Paper*. SAE International. DOI:10.4271/2005-01-3602.
5. Mohammadpour J, Franchek M and Grigoriadis K. A survey on diagnostic methods for automotive engines. *International Journal of Engine Research* 2012; 13(1): 41–64.
6. P Jones JC and Muske KR. Model-based obd for three-way catalyst systems. SAE International. DOI:https://doi.org/10.4271/2004-01-0639.
7. Ye S, Yap YH, Kolaczkowski ST et al. Catalyst light-off experiments on a diesel oxidation catalyst connected to a diesel engine-methodology and techniques. *Chemical Engineering Research and Design* 2012; 90(6): 834 – 845.
8. Schultz R and Meckl PH. Light-off temperature shift for catalyzed diesel particulate filter on-board diagnostics. In *SAE Technical Paper*. SAE International. DOI:10.4271/2012-01-1248.
9. Bartley GJ. Identifying limiters to low temperature catalyst activity. In *SAE Technical Paper*. SAE International. DOI:10.4271/2015-01-1025.

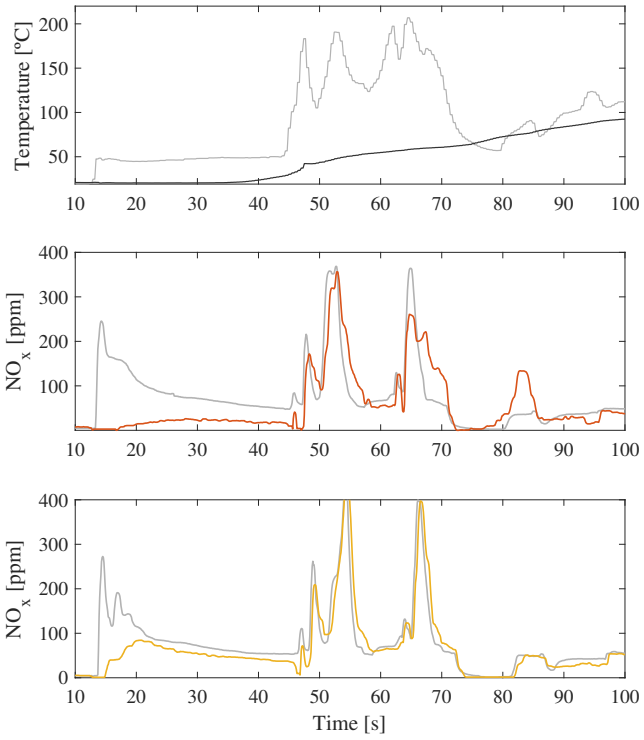

Figure 15. Measured effect of ageing on the NO_x accumulation process at the cold starting phase of the WLTC. Top plot: Upstream temperature Downstream temperature. Medium (new) and bottom (aged) plots: $NO_{x,in}$ $NO_{x,out,new}$ $NO_{x,out,aged}$

10. Henry C, Currier N, Ottinger N et al. Decoupling the interactions of hydrocarbons and oxides of nitrogen over diesel oxidation catalysts. In *SAE 2011 World Congress & Exhibition*. SAE International. DOI:10.4271/2011-01-1137.
11. Tourlonias P and Koltsakis G. Model-based comparative study of Euro 6 diesel aftertreatment concepts, focusing on fuel consumption. *International Journal of Engine Research* 2011; 12(3): 238–251.
12. Sampara CS, Bissett EJ, Chmielewski M et al. Global kinetics for platinum diesel oxidation catalysts. *Industrial & Engineering Chemistry Research* 2007; 46(24): 7993–8003.
13. Kryl D, Kocí P, Kubícek M et al. Catalytic converters for automobile diesel engines with adsorption of hydrocarbons on zeolites. *Industrial & engineering chemistry research* 2005; 44(25): 9524–9534.
14. Sampara CS, Bissett EJ and Chmielewski M. Global kinetics for a commercial diesel oxidation catalyst with two exhaust hydrocarbons. *Industrial & Engineering Chemistry Research* 2008; 47(2): 311–322.
15. Tanaka Y, Hihara T, Nagata M et al. Modeling of diesel oxidation catalyst. *Industrial & engineering chemistry research* 2005; 44(22): 8205–8212.
16. Matsumoto A, Furui K, Ogiso M et al. Model-based OBD logic utilizing adsorption and desorption model of NH3 in SCR catalyst. In *SAE Technical Paper*. SAE International. DOI: 10.4271/2016-01-0960.
17. Figura J, Pekar J, Krejza P et al. NO2/NOx ratio and NH3 storage estimation of automotive SCR multi-brick systems. In *SAE Technical Paper*. SAE International. DOI:10.4271/2017-01-0972.
18. Li J, Szailer T, Watts A et al. Investigation of the impact of real-world aging on diesel oxidation catalysts. *SAE Int J Engines* 2012; 5: 985–994. DOI:10.4271/2012-01-1094.
19. Ahari H, Zammit M, Cattani L et al. Cause and effect of reversible deactivation of diesel oxidation catalysts. In *SAE Technical Paper*. SAE International. DOI:10.4271/2014-01-1518.
20. Nakane T, Ikeda M, Hori M et al. Investigation of the aging behavior of oxidation catalysts developed for active DPF regeneration systems. In *SAE Technical Paper*. SAE International. DOI:10.4271/2005-01-1759.
21. Guardiola C, Pla B, Mora J et al. Control oriented model for diesel oxidation catalyst diagnosis. *IFAC-PapersOnLine* 2015; 48(15): 427 – 433.
22. Chen P and Wang J. Control-oriented model for integrated diesel engine and aftertreatment systems thermal management. *Control Engineering Practice* 2014; 22: 81–93.
23. Kim YD and Kim WS. Re-evaluation and modeling of a commercial diesel oxidation catalyst. *Industrial & Engineering Chemistry Research* 2009; 48(14): 6579–6590.
24. Guardiola C, Dolz V, Pla B et al. Fast estimation of diesel oxidation catalysts inlet gas temperature. *Control Engineering Practice* 2016; 56: 148–156.
25. Sampara CS, Bissett EJ and Assanis D. Hydrocarbon storage modeling for diesel oxidation catalysts. *Chemical Engineering Science* 2008; 63: 5179–5192.
26. Kim YW, Van Nieuwstadt M, Stewart G et al. Model predictive control of DOC temperature during DPF regeneration. In *SAE Technical Paper*. SAE International. DOI:10.4271/2014-01-1165.
27. Ruetten O, Pischinger S, Kuepper C et al. Catalyst aging method for future emissions standard requirements. In *SAE Technical Paper*. SAE International. DOI:10.4271/2010-01-1272.
28. Sutjiono R, Tayal P, Zhou K et al. Real-time on-board indirect light-off temperature estimation as a detection technique of diesel oxidation catalyst effectiveness level. In *SAE Technical Paper*. SAE International. DOI:10.4271/2013-01-1517.
29. Arvajova A, Koci P, Schmeisser V et al. The impact of CO and C3H6 pulses on ptox reduction and no oxidation in a diesel oxidation catalyst. *Applied Catalysis B: Environmental* 2016; 181: 644 – 650.
30. Mallamo F, Longhi S, Millo F et al. Modeling of diesel oxidation catalysts for calibration and control purpose. *International Journal of Engine Research* 2014; 15(8): 965–979.

Appendix: Model application to the WLTC

Model application figures are presented in this appendix for new and aged DOC units in Figures 16 and 17, respectively.

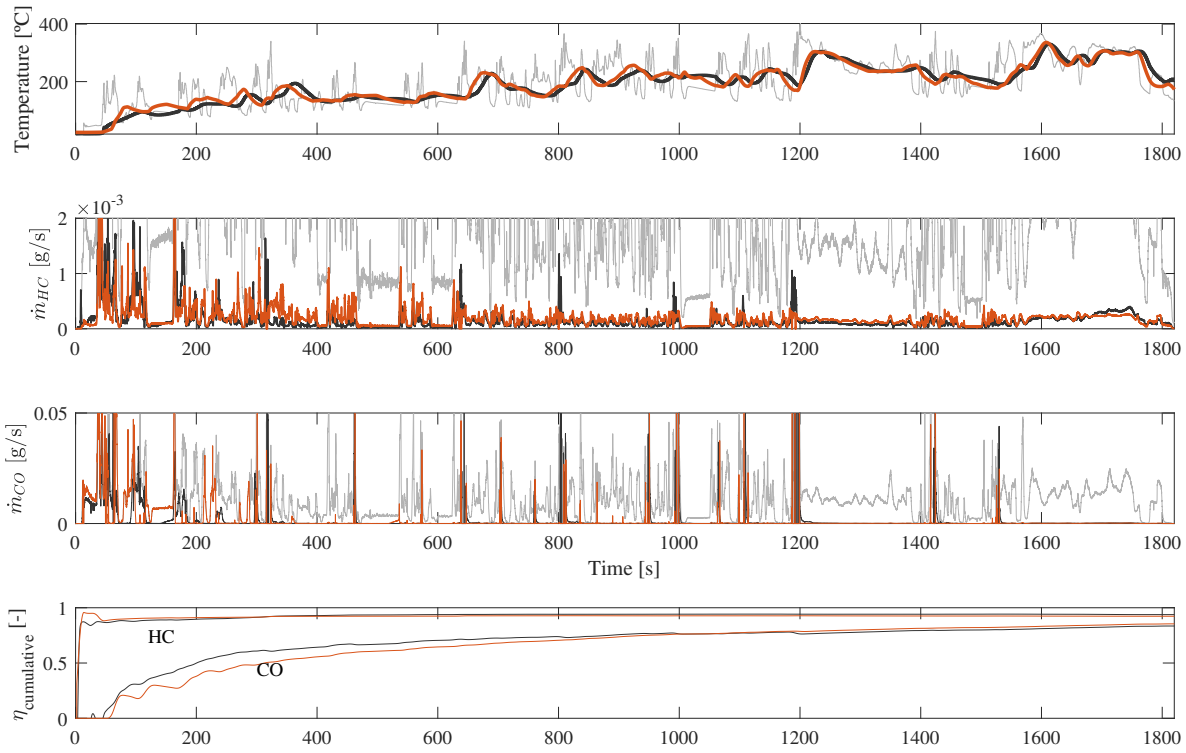

Figure 16. New DOC model results in a WLTC. Upper plots: Upstream measurements Downstream measurements Downstream model. Bottom plot: Cumulative efficiency from measurements Cumulative efficiency from model.

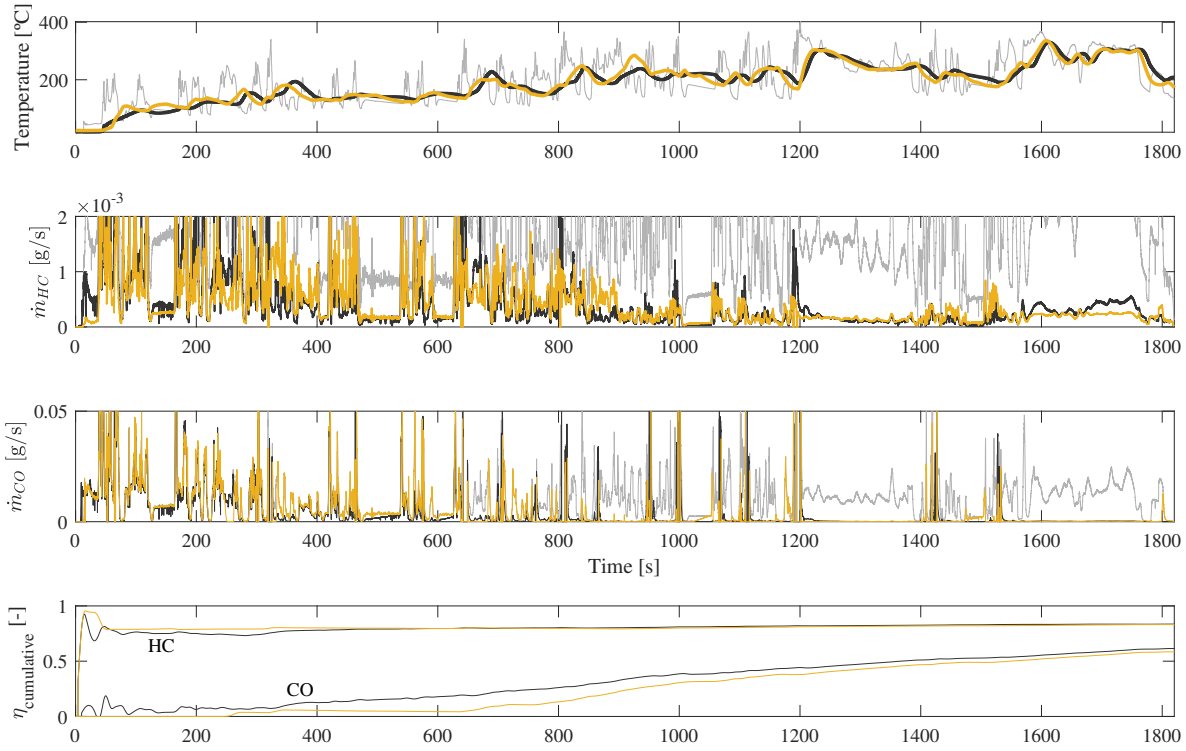

Figure 17. Aged DOC model results in a WLTC. Upper plots: Upstream measurements Downstream measurements Downstream model. Bottom plot: Cumulative efficiency from measurements Cumulative efficiency from model.